JCI The Journal of Clinical Investigation

Retinoblastoma protein prevents enteric nervous system defects and intestinal pseudo-obstruction

Ming Fu, … , J. William Harbour, Robert O. Heuckeroth

J Clin Invest. 2013;123(12):5152-5164. https://doi.org/10.1172/JCI67653.

Research Article **Gastroenterology**

The retinoblastoma 1 (RB1) tumor suppressor is a critical regulator of cell cycle progression and development. To investigate the role of RB1 in neural crest–derived melanocytes, we bred mice with a floxed *Rb1* allele with mice expressing *Cre* from the tyrosinase (*Tyr*) promoter. *TyrCre*$^{+}$*;Rb1*$^{fl/fl}$ mice exhibited no melanocyte defects but died unexpectedly early with intestinal obstruction, striking defects in the enteric nervous system (ENS), and abnormal intestinal motility. Cre-induced DNA recombination occurred in all enteric glia and most small bowel myenteric neurons, yet phenotypic effects of *Rb1* loss were cell-type specific. Enteric glia were twice as abundant in mutant mice compared with those in control animals, while myenteric neuron number was normal. Most myenteric neurons also appeared normal in size, but NO-producing myenteric neurons developed very large nuclei as a result of DNA replication without cell division (i.e., endoreplication). Parallel studies in vitro found that exogenous NO and *Rb1* shRNA increased ENS precursor DNA replication and nuclear size. The large, irregularly shaped nuclei in NO-producing neurons were remarkably similar to those in progeria, an early-onset aging disorder that has been linked to RB1 dysfunction. These findings reveal a role for RB1 in the ENS.

Retinoblastoma protein prevents enteric nervous system defects and intestinal pseudo-obstruction

Ming Fu,[1] Solange Landreville,[2] Olga A. Agapova,[2] Luke A. Wiley,[2] Michael Shoykhet,[1] J. William Harbour,[2,3] and Robert O. Heuckeroth[1,4]

[1]Department of Pediatrics and [2]Department of Ophthalmology and Visual Sciences, Washington University School of Medicine in St. Louis, St. Louis, Missouri, USA. [3]Bascom Palmer Eye Institute, University of Miami Miller School of Medicine, Miami, Florida, USA. [4]Department of Developmental, Regenerative and Stem Cell Biology, Washington University School of Medicine in St. Louis, St. Louis, Missouri, USA.

The retinoblastoma 1 (RB1) tumor suppressor is a critical regulator of cell cycle progression and development. To investigate the role of RB1 in neural crest–derived melanocytes, we bred mice with a floxed *Rb1* allele with mice expressing *Cre* from the tyrosinase (*Tyr*) promoter. *TyrCre*$^+$*;Rb1*$^{fl/fl}$ mice exhibited no melanocyte defects but died unexpectedly early with intestinal obstruction, striking defects in the enteric nervous system (ENS), and abnormal intestinal motility. Cre-induced DNA recombination occurred in all enteric glia and most small bowel myenteric neurons, yet phenotypic effects of *Rb1* loss were cell-type specific. Enteric glia were twice as abundant in mutant mice compared with those in control animals, while myenteric neuron number was normal. Most myenteric neurons also appeared normal in size, but NO-producing myenteric neurons developed very large nuclei as a result of DNA replication without cell division (i.e., endoreplication). Parallel studies in vitro found that exogenous NO and *Rb1* shRNA increased ENS precursor DNA replication and nuclear size. The large, irregularly shaped nuclei in NO-producing neurons were remarkably similar to those in progeria, an early-onset aging disorder that has been linked to RB1 dysfunction. These findings reveal a role for RB1 in the ENS.

Introduction

Chronic intestinal pseudo-obstruction (CIPO) is the clinical indication for 9 percent of small bowel transplants (1), yet the etiology for these disorders remains poorly understood. CIPO is diagnosed when bowel motility defects cause functional, but not mechanical, obstruction, leading to abdominal distension, pain, malnutrition, and, in severe cases, dependence on parenteral nutrition or intestinal transplantation for survival. It is likely that diverse genetic, infectious, autoimmune, metabolic, and toxic insults all contribute to CIPO etiology.

Intestinal motility and many other aspects of bowel function are controlled by an interconnected intrinsic network of neurons and glia called the enteric nervous system (ENS) (2–4). The ENS forms from neural crest–derived cells that migrate through fetal bowel, proliferate extensively, and then exit the cell cycle and differentiate into many different neuronal subtypes (5–7). Defects in specific types of enteric neurons may cause life-threatening disease, and, like in the central nervous system, neurons in the ENS must be present in the proper ratios and with correct patterning for the bowel to work well. Signals that control ENS precursor proliferation and cell cycle exit are incompletely understood. Furthermore, the ENS can be damaged in many ways, often with preferential effects on NO-producing enteric neurons that inhibit bowel contraction (8). There are also regional differences in the susceptibility of enteric neurons to damage that are not well understood (9).

We initially intended to develop a model of melanoma by deleting the tumor suppressor retinoblastoma 1 (*Rb1*) in melanocytes, another neural crest derivative. *Rb1* is frequently inactivated in human cancer (10) and critically regulates cell division and development (11–16). Cyclin-dependent kinases promote cell division by reversibly inactivating RB1 via a hierarchical series of phosphorylation events and sequential conformational changes (12, 13). The best understood function of RB1 is to induce cell cycle exit by preventing cells from entering S phase (17), but it also participates in cell cycle checkpoints in S and G_2/M phases (14). RB1 is important not only for tumor suppression but also for development, terminal differentiation, and tissue homeostasis (15), with mutations causing tissue-specific defects (18, 19). We had previously demonstrated that RB1 couples cell cycle exit with terminal differentiation in melanocytes (20) and therefore crossed mice carrying a tyrosinase-Cre (*TyrCre*) transgene with mice harboring floxed *Rb1* alleles. This *TyrCre* transgene is expressed not only in the melanocyte lineage, but also in the developing ENS. We discovered that *Rb1* inactivation in the ENS led to a progressive, fatal, and very unusual defect in a subset of myenteric neurons that produce NO. These cells undergo endoreplication and develop giant, irregularly shaped nuclei similar to those seen in progeria. Strikingly, although *Rb1* is also deleted in enteric glia and other types of enteric neurons, these cells do not undergo endoreplication, highlighting the complexity of cell cycle regulation and differences in *Rb1* dependence of distinct cell types within the ENS lineage.

Results

Rb1 loss in the ENS causes a severe intestinal motility disorder and early death. *Rb1*$^{fl/fl}$ mice were bred with *TyrCre* mice, and at P8, the resulting *TyrCre*$^+$*;Rb1*$^{fl/fl}$ mice (*Rb1* conditional KO [cKO] mice; Figure 1A) were present at a normal Mendelian ratio (*Rb1*$^{+/+}$, 19%; heterozygous *Rb1* cKO, 59%; *Rb1* cKO, 22%; χ^2 test $P = 0.5$, $n = 37$ *Cre*$^+$ mice analyzed). However, the P8 *Rb1* cKO mice were smaller than littermates and

Authorship note: J. William Harbour and Robert O. Heuckeroth are co–senior authors.

Conflict of interest: The authors have declared that no conflict of interest exists.

Citation for this article: *J Clin Invest.* 2013;123(12):5152–5164. doi:10.1172/JCI67653.

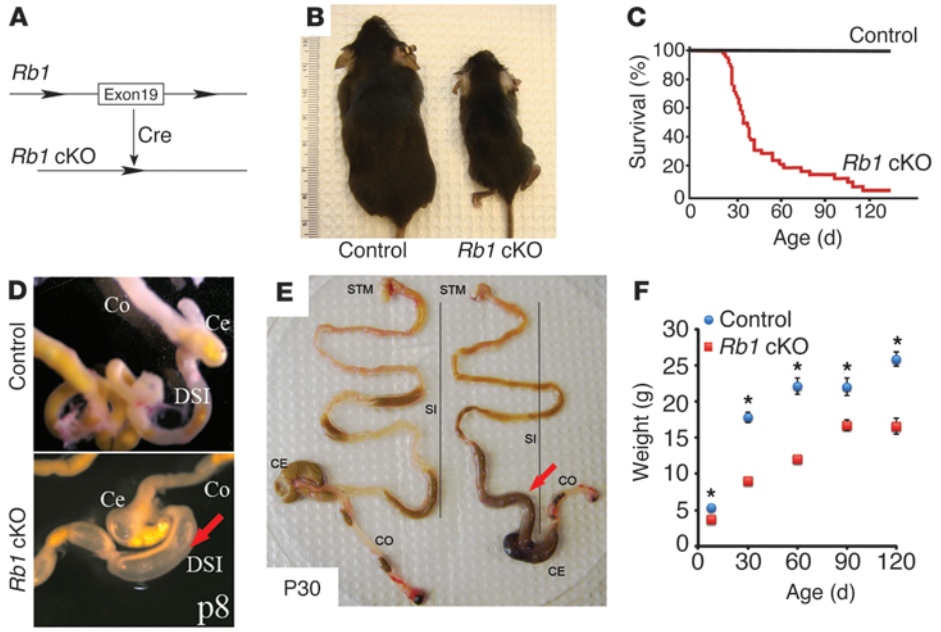

Figure 1
Rb1 cKO mice gain weight slowly and die of intestinal pseudo-obstruction. (**A**) LoxP sites surrounding *Rb1* exon 19 led to inactivation by tyrosinase promoter–driven Cre-recombinase. (**B**) Adult *Rb1* cKO mice were smaller than WT littermates (ruler depicts centimeters). (**C**) *Rb1* cKO mice die prematurely; 50% of mice were dead by P30. (**D** and **E**) DSIs of *Rb1* cKO mice become dilated (red arrows) and colons have hard dark stool scybala at (**D**) P8 and (**E**) P30. Ce, cecum; Co, colon; STM, stomach; SI, small intestine; DSI, distal small bowel. (**F**) *Rb1* cKO mice grow slowly (control, $n = 33$; Rb1 cKO, $n = 33$). $^*P < 0.05$.

continued to grow poorly (Figure 1, B and F). By P21, *Rb1* cKO mice were present at a lower ratio than expected (*Rb1*$^{+/+}$, 29%; heterozygous *Rb1* cKO, 55%; *Rb1* cKO, 16%; χ^2 test $P < 0.001$, $n = 806$ *Cre*$^+$ mice analyzed). By P30, 50% of *Rb1* cKO mice had died (Figure 1C). To determine the cause of death, *Rb1* cKO animals were subjected to necropsy for gross and histopathologic examination of all major organs. We did not observe any melanocyte defects or tumors, similar to results of Tonks et al. (21), but early death prevented the study of late-onset melanoma. The only abnormality detected was marked dilation of the distal small intestine (DSI) with intraluminal stool or air accumulation and contraction of the more distal bowel. This phenotype was evident in some *Rb1* cKO mice by P8 (Figure 1D; $n = 2$ out of 4 examined) and in 70% of mice at 30 days or older (Figure 1E; WT, $n = 14$; *Rb1* cKO, $n = 21$), indicating a progressive bowel motility defect that likely underlies the poor growth and early death in these mice. Heterozygous *TyrCre*$^+$;*Rb1*$^{+/fl}$ mice were healthy without abnormal phenotype at all ages examined (data not shown). Because *TyrCre* mice express *Cre* in neural crest derivatives, including the ENS (22–24), we hypothesized that this *Rb1* mutation caused ENS defects.

Rb1 cKO mouse myenteric plexus neurons undergo DNA replication without mitosis. The gross intestinal phenotype in *Rb1* cKO mice with dilated proximal and relatively narrow distal bowel was reminiscent of human Hirschsprung disease, in which the ENS is absent from the distal bowel. However, histopathologic examination of mice at various ages from P0 to adulthood did not reveal the characteristic distal bowel aganglionosis of Hirschsprung disease ($n = 33$ mice examined). Since the ENS was present, we next considered the possibility that one or more cell types within the ENS were abnormal in *Rb1* cKO mice. To test this hypothesis, adult mouse whole-mount preparations of the bowel muscle layers containing the myenteric plexus were stained with antibodies against HuC/D for visualizing neuronal cell bodies, TuJ1 for visualizing neurites, and S100 or SOX10 for visualizing enteric glia (Figure 2, A–H). At P30, SOX10 and S100 antibodies labeled exactly the same cells (100% overlap) in WT and *Rb1* cKO mice (Supplemental Figure 1; supplemental material available online with this article; doi:10.1172/JCI67653DS1). Quantitative analysis of *Rb1* cKO mice demonstrated a normal density of myenteric neurons in the distal small bowels and colons but a significant increase in enteric glial density compared with that in WT mice (Figure 2, I and J). Interestingly, there were also many exceptionally large neurons (but not glia) in the distal small bowels of *Rb1* cKO mice that were not observed in WT animals (Figure 2, D and H). Large neurons were seen, but were uncommon, in the colons of *Rb1* cKO animals. To further investigate nuclear morphology in distal small bowel, we used an antibody against the nuclear matrix proteins lamin A/C (LMNA/C) in combination with HuC/D and the DNA dye DRAQ5 (Figure 3, A–D). This staining demonstrated very large nuclei with complex internal and external LMNA/C-containing lamina. In some cases, LMNA/C "vesicles" are contained within a larger nuclear lamina, and in others, smaller LMNA/C "vesicles" are adjacent to or contiguous with a larger nucleus (see Supplemental Figure 2 and Supplemental Videos 1–6). In addition to the unusual nuclear lamina structures, the large nuclear size suggested that these neurons might be replicating DNA without cell division (i.e., endoreplication). Alternatively, nuclear enlargement might be independent of DNA replication. To distinguish between these possibilities, we first attempted fluorescence-activated cell sorting and fluorescence in situ hybridization to estimate DNA content, but these techniques were not successful on the whole-mount preparations required for these studies. Therefore, we used confocal microscopy and integrated DRAQ5 staining intensity to estimate DNA content and measure nuclear volume. For these analyses, we used a lamin B2 antibody that stained the nuclear lamina of myenteric neurons but not those of other cells in the whole-mount preparations (Supplemental Figure 3). This analysis demonstrated that nuclear volume in *Rb1* cKO mice was up to 32-fold larger than that in WT mice and nuclear volume was directly proportional to DNA content (Figure 3E), consistent with endoreplication in *Rb1* mutant myenteric neurons. To validate the hypothesis that *Rb1* mutant myenteric neurons continue to replicate DNA after control myen-

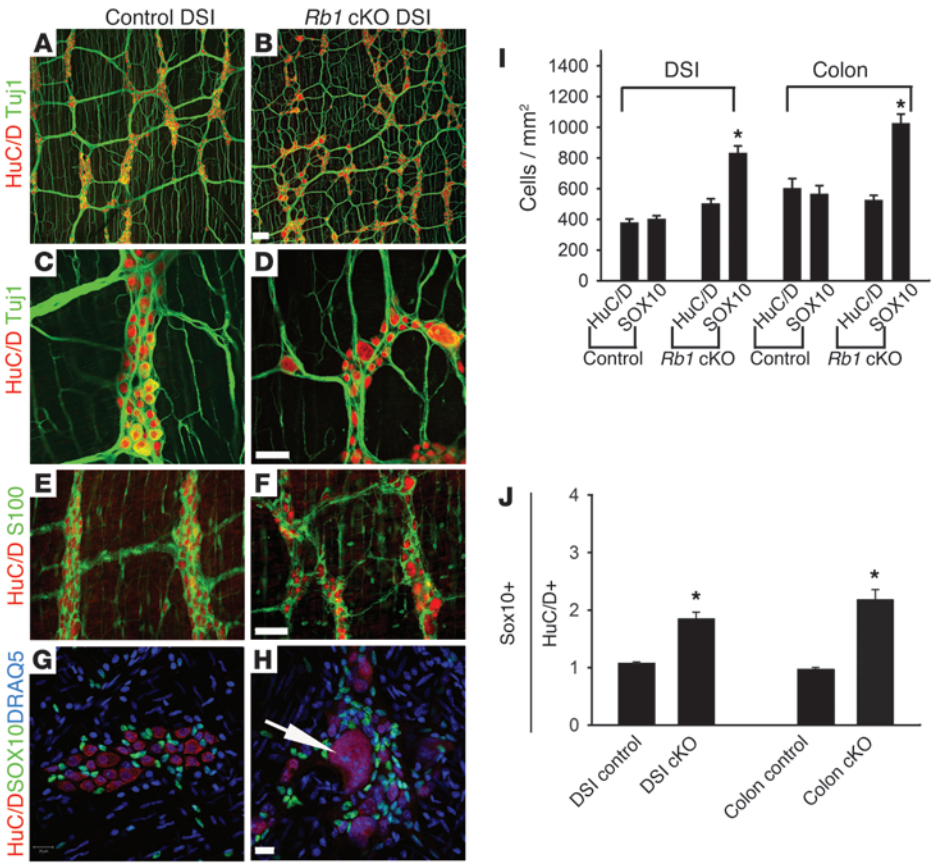

Figure 2

Rb1 cKO mice have disorganized myenteric ganglia with giant neurons and increased enteric glia. (**A**–**D**) Whole-mount preparations of the myenteric plexus stained with antibodies to HuC/D (red, neuronal marker) and Tuj1 (green, neuron-specific bIII tubulin) demonstrated some very large myenteric neurons in *Rb1* cKO mice. (**E** and **F**) S100 (green, glia cytoplasm marker) and HuC/D (red) or (**G** and **H**) SOX10 (green, glial protein), DRAQ5 (blue, DNA dye), and HuC/D (red) immunohistochemistry showed an increased ratio of glia to neurons and normal glial cell size in ganglia with very large neurons (white arrow in **H**). (**A** and **B**) Ganglia also appear disorganized in *Rb1* cKO mice. (**I**) Quantitative analysis demonstrated approximately twice as many enteric glia in the distal small bowels and colons of *Rb1* cKO mice compared with those in controls. Neuron numbers were equal in *Rb1* cKO and control mice. (**J**) We confirmed an increased glia to neuron ratio by counting cells within the same field of view in the distal small bowel and colon. Scale bar: 100 μm (**A** and **B**); 50 μm (**C**–**F**); 20 μm (**G** and **H**). *$P < 0.05$ versus control. n > 1,000 neurons and >2,000 glia per analysis.

teric neurons have exited the cell cycle, we injected mice with BrdU daily from P9 to P16 and analyzed the enteric neurons at P20 with an antibody against BrdU in conjunction with PGP9.5 (neuronal) and SOX10 (glial) immunohistochemistry. This revealed a marked increase in BrdU incorporation in neurons of *Rb1* cKO mice compared with those in WT mice (Figure 4, A, B, and E), indicating that *Rb1* mutant myenteric neurons continue to replicate DNA at this age, whereas WT myenteric neurons have ceased DNA synthesis. Similarly, staining with an antibody against the proliferation marker Ki67 (Figure 4, C, D, and F) showed that *Rb1* mutant myenteric neurons remained in the cell cycle, whereas WT myenteric neurons had exited the cell cycle at this age. Some SOX10$^+$ enteric glial cells were also positive for Ki67 and BrdU staining, but the percentages of positive cells did not differ between *Rb1* cKO and WT mice (Figure 4, E and F).

Nuclear enlargement is not likely to be associated with neuronal cell death, since we were unable to detect TUNEL-positive cells in the myenteric plexuses of *Rb1* cKO or control mice at P30, P50, or P60 (data not shown). We also did not find evidence of DNA damage in myenteric neurons by staining with γ-H2AX antibody (Supplemental Figure 4).

NO-producing distal small bowel myenteric neurons are selectively affected by RB1 loss. We observed a marked variability in the nuclear size of myenteric plexus neurons in the distal small bowel of *Rb1* cKO mice and hypothesized that RB1 loss may selectively affect certain types of myenteric neurons. If this were the case, then the affected cell type would likely be an abundant one, such as NO-producing inhibitory motor neurons or calretinin-expressing excitatory motor neurons. To evaluate NO-producing cells, we used nicotinamide adenine dinucleotide phosphate diaphorase (NADPH-d) staining on whole-mount preparations of the distal small bowel myenteric plexus at P8 and P30 (Figure 5). At P30, many NADPH-d–expressing neurons exhibited giant nuclei, whereas very few giant nuclei were observed at P8, suggesting that postnatal DNA replication without mitosis in NO-producing myenteric neurons leads to progressive nuclear enlargement. This is consistent with the observation

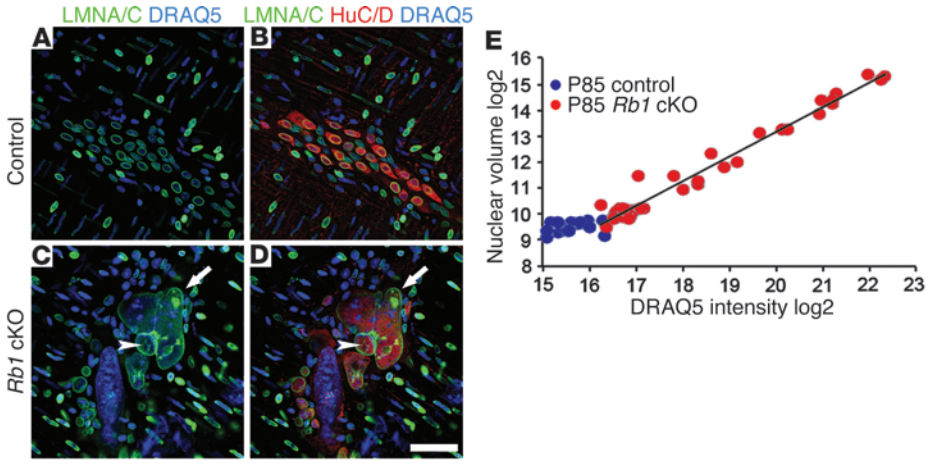

Figure 3
Nuclear size correlates with DNA content in myenteric neurons of *Rb1* cKO mice. Immunohistochemistry for LMNA/C (green, nuclear lamina), HuC/D (red), and DRAQ5 (blue) demonstrated distal small bowel myenteric neurons with very large nuclei (arrow) and irregular shapes (arrowhead) (**C** and **D**) in *Rb1* cKO mice but (**A** and **B**) not in WT mice. (**E**) Integrated DRAQ5 fluorescence intensity values for nuclei (log_2) versus nuclear volume (log_2) in distal small bowel myenteric neurons of P85 control (blue dots) and *Rb1* cKO mice (red dots) demonstrated a linear correlation between nuclear volume and DNA content in *Rb1* cKO nuclei and confirmed that many nuclei are much larger than normal in *Rb1* cKO mice. Eight to 10 different Z-stacks per animal were analyzed. Scale bar: 50 μm.

that the density of NO-producing neurons in the distal small bowels and colons of *Rb1* cKO mice was normal (WT DSI, 63 ± 7 per mm^2; *Rb1* cKO, 55 ± 8.5 per mm^2, $P = 0.3$; WT colon, 98 ± 13 per mm^2; *Rb1* cKO colon, 109 ± 12 per mm^2, $P = 0.4$).

Further, we performed immunohistochemical staining of the small bowel and colon with antibodies against neuronal NO synthase (nNOS), PGP9.5 (stains all neurons), and calretinin (stains excitatory motor neurons), along with histochemical staining for NADPH-d, and performed quantitative analysis (Figure 6). The giant nuclei (up to 7 times larger than normal cross-sectional area) were limited to NO-producing neurons in the distal small bowels of *Rb1* cKO mice, whereas calretinin-expressing neurons in the same region of the bowel had nuclei of normal size (Figure 6, A, B, E–G, and I). In contrast, there were very few PGP9.5$^+$ neurons or NADPH-d–expressing neurons in the colon with nuclei that were larger than normal (Figure 6, C, D, and H). Enteric glia in *Rb1* cKO mice also had nuclei with normal appearance. These findings demonstrate differential effects on the size of neuronal nuclei in *Rb1* cKO mice and selective vulnerability of distal small bowel NO-producing neurons to RB1 loss.

One possible explanation for these findings is that Cre may be expressed selectively in NO-producing small bowel myenteric neurons. To evaluate this possibility, we studied the pattern of Cre expression in *TyrCre* mice by crossing them with a Cre-dependent enhanced yellow fluorescent protein (EYFP) reporter mouse line. Quantitative analysis at P30 demonstrated Cre-dependent EYFP expression in 100% of SOX10$^+$ enteric glia, 62% of distal small bowel myenteric neurons, 17% of colon myenteric neurons, 93% of distal small bowel nNOS-expressing myenteric neurons, 90% of distal small bowel calretinin$^+$ myenteric neurons, 76% of colon nNOS$^+$ myenteric neurons, and 80% of colon calretinin$^+$ myenteric neurons (Supplemental Figure 5). We also noted that, in our mice, 12% of colon myenteric neurons had nNOS immunoreactivity and 12% had calretinin immunoreactivity, lower percentages than previously reported in BALB/c mice (25). Finally, we performed immunohistochemistry for PHOX2B in these mice at E10.5 and E11.5 (Supplemental Figure 6) and found that Cre-induced recombination occurred with some, but not all, ENS precursors by E10.5 and in almost all ENS precursors by E11.5. Thus, differential effects of RB1 loss on cells of the ENS cannot be explained on the basis of asymmetric *Cre* expression, suggesting that NO-producing neurons are selectively affected by RB1 loss. We also tested the possibility that differential expression of *Rb1* family members p130 and p107 could account for the selective effects on NO-producing neurons but found that p107 was expressed at low levels in WT and *Rb1* cKO myenteric neurons (Figure 7). In contrast, p130 was not detected in WT myenteric neurons but was present in all *Rb1* cKO myenteric neurons, suggesting that although changes in p130 protein abundance occur and p107 is present in myenteric neurons, the expression of these proteins does not account for the differential effects of *Rb1* mutation in myenteric neuron subpopulations or substitute for RB1.

NO causes proliferation of ENS precursors in vitro. The striking effect of the *Rb1* mutation on NO-producing neurons and the limited effect of this mutation on other enteric neuron types raised the possibility that NO itself influences DNA replication in ENS precursors when RB1 activity is low. To test this hypothesis, we generated a lentivirus that silences *Rb1* and confirmed activity using dissociated E12.5 bowel and quantitative real-time RT-PCR (qRT-PCR) (Supplemental Figure 7). E12.5 mouse embryonic midgut slices (300- to 400-μm thick) were then cultured with GDNF to induce ENS precursors to migrate onto the dish and treated with *Rb1* shRNA lentivirus or a control shRNA-expressing virus with or without added NO donor (DETA NONOate). Virus-infected ENS precursors identified by GFP and RET expression were analyzed 48 hours later using phospho-histone 3 (PH3) immunohistochemistry (Figure 8). These studies demonstrated that silencing *Rb1* and the chemical NO donor DETA NONOate each independently increased the percentage of RET-expressing cells that were PH3$^+$ (Figure 8E, 2-way ANOVA, $P < 0.001$). Furthermore, the NO donor induced the generation of some RET$^+$ cells with very large nuclei when *Rb1* was silenced (Figure 8J), even over 2 days in culture. These data suggest that the striking phenotype of NO-producing myenteric neurons in *Rb1* cKO mice is induced by a combination of *Rb1* loss and high NO levels.

Intestinal motility is abnormal in Rb1 cKO mice. The preceding analysis demonstrated that *Rb1* cKO mice die early, develop distal small bowel dilation, and have very large, unusual NO-producing neu-

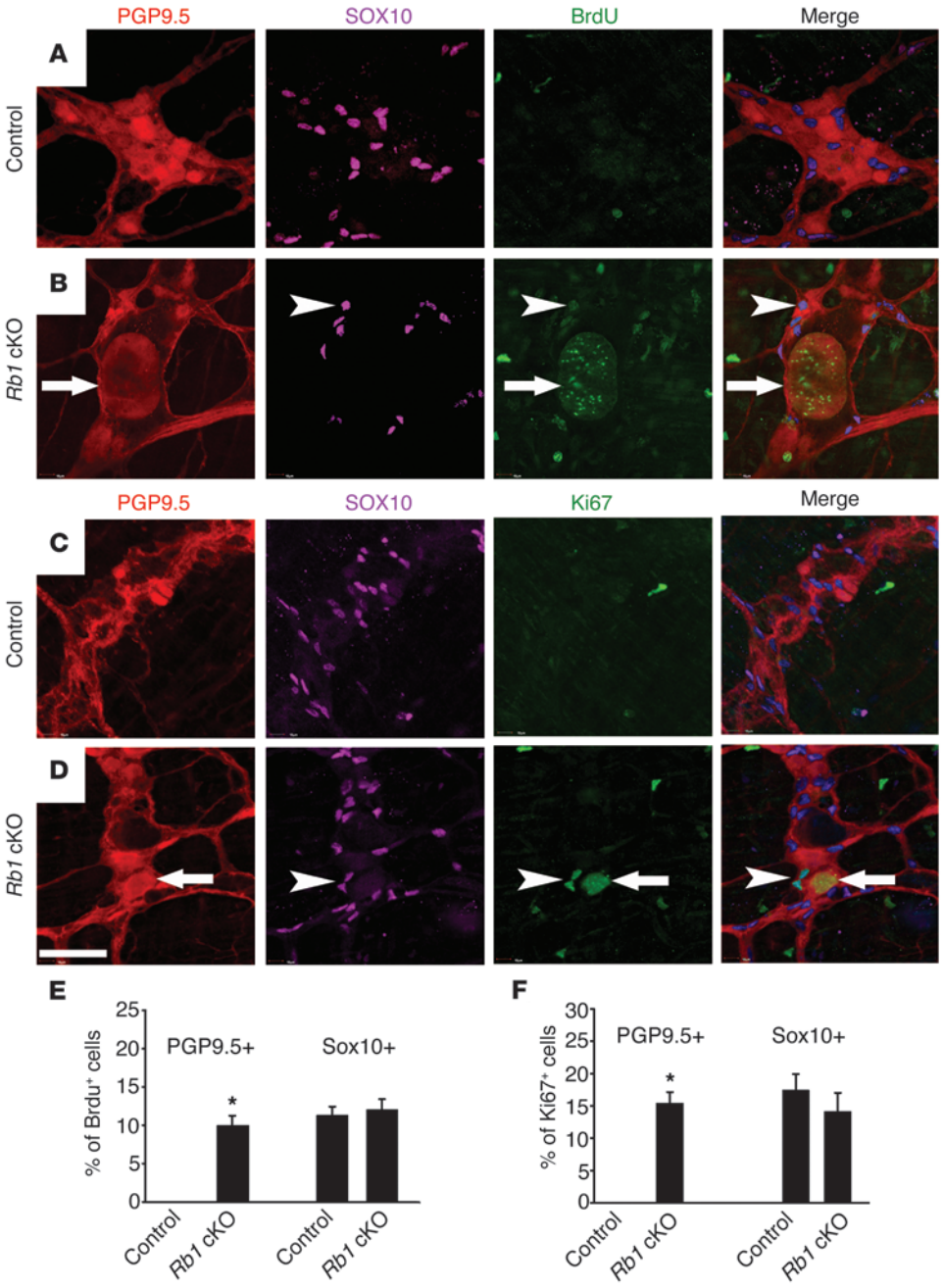

Figure 4

Rb1 cKO mice have an increased number of BrdU+ and Ki67+ myenteric neurons in the distal small bowel, but BrdU+ or Ki67+ myenteric neurons were not detected in controls. Mice were injected with BrdU daily from P9 to P16 and then sacrificed at P20. (**A**–**D**) Immunohistochemistry for PGP9.5 (red), SOX10 (purple), BrdU (green), and Ki67 (green) was used to detect neurons, glia, DNA synthesis, and cycling cells, respectively. BrdU+ and Ki67+ neurons and glia were readily detectable in *Rb1* cKO mice. (**B**) The arrows highlight a large neuron with BrdU incorporation into the nucleus. (**D**) The arrows highlight a Ki67+ neuron. Arrowheads highlight (**B**) BrdU+ and (**D**) Ki67+ glia. BrdU+ and Ki67+ neurons were not detected in WT mice. (**E** and **F**) Quantitative analysis (n = 200 cells per bar). Scale bar: 50 μm. *P < 0.05 versus control.

rons in the region in which the bowel is dilated. We hypothesized that this distal small bowel dilation occurred, at least in part, because these neurons produced excess NO that caused smooth muscle relaxation. An additional potential mechanism is that small bowel dilation occurred because colonic dysfunction prevented luminal contents from exiting the small bowel and entering the colon. If small bowel dilation was due to intrinsic defects, the distal small bowels of *Rb1* cKO mice should remain dilated and contract poorly even when separated from the colons. To test this hypothesis, we examined spontaneous contractions of the ilea from 3 WT and 3 *Rb1* cKO mice using an oxygenated organ bath. The WT small bowel contracted vigorously (Supplemental Video 7), but *Rb1* cKO small bowel was dilated (Figure 9) and contracted very little (Supplemental Video 8), even when separated from the colon. Direct analysis of distal small bowel muscle layer NO synthesis, based on conversion of [^{3}H]-arginine to citrulline (26), also demonstrated 2.8-fold more NO synthesis in *Rb1* cKO mice compared with that in WT mice (WT, 0.69 ± 0.16 cpm/mg/min, n = 4; *Rb1* cKO, 1.93 ± 0.34 cpm/mg/min, n = 3, P = 0.016). For *Rb1* cKO animals, the ilea contracted after addition of the NO synthesis inhibitor, L-NAME, and motility increased (Figure 9D and Supplemental Video 10), consistent with the hypothesis that NO actively inhibited contraction in the *Rb1* cKO ileum but bowel contraction was less obvious after L-NAME addition to WT distal small bowel (Supplemental Video 9). Collectively these data show that there are serious motility problems in the distal small

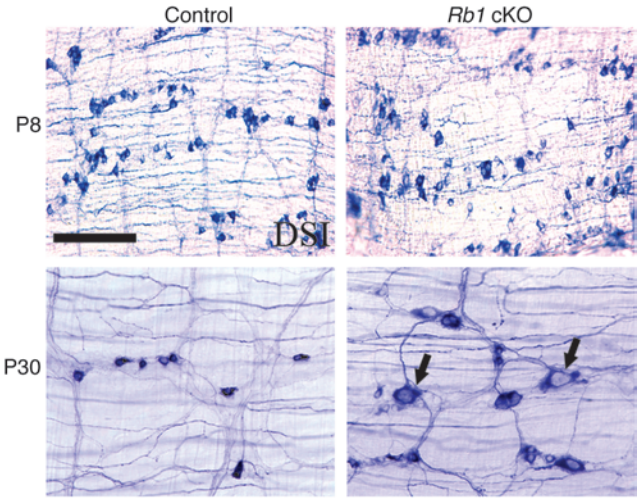

Figure 5
NADPH-d–expressing myenteric neurons with large nuclei appeared as mice aged. Distal small bowel myenteric plexus neurons were visualized with the NADPH-d method that stains NO-producing neurons. Large neurons were easy to find after P30 but not present at P8. Arrows highlight NADPH-d$^+$ neurons in *Rb1* cKO mice that are larger than normal. Scale bar: 100 μm.

bowels of *Rb1* cKO mice that could cause poor growth and premature death. Interestingly, colon contractility patterns were also abnormal in *Rb1* cKO mutant mice. In contrast to the control animals, in which an artificial stool pellet was propelled distally through the colon (n = 3; Supplemental Video 11), an artificial stool pellet inserted into the proximal colons of *Rb1* cKO mice was propelled proximally (n = 3; Supplemental Video 12 and Figure 10). Collectively, these findings demonstrate severe bowel motility defects and are consistent with the hypothesis that a progressive intestinal pseudo-obstruction phenotype caused death at between 30 and 120 days of age in *Rb1* cKO mice.

Discussion

We discovered an important and previously unsuspected role for RB1 in the ENS. Mice with conditional, biallelic *Rb1* deletion in the ENS appear healthy at birth but grow slowly and die as young adults. This early mortality appears due to marked distal small bowel distension and relative contraction of the colon, consistent with partial obstruction, as a result of ENS dysfunction. When we first observed the phenotype, we considered the possibility that *Rb1* cKO mice had distal bowel aganglionosis similar to that in human Hirschsprung disease, but many mice lived longer than would be expected if there were a region without ganglion cells. Furthermore, although there are rare reports of children with Hirschsprung disease and retinoblastoma, this probably results from contiguous gene deletion that includes *EDNRB* at 13q22 and *RB1* at 13q14.2 (27, 28). Instead, we discovered that *Rb1* cKO mice had a normal number of myenteric neurons in the small bowel and colon and a 2-fold increase in enteric glia. We also found a subset of NO-producing neurons with very large, irregularly shaped nuclei primarily in the distal small bowel. Analysis of contractility in isolated bowel segments demonstrated severe motility defects in both small bowels and colons of *Rb1* cKO mice.

The etiology of intestinal motility problems in *Rb1* cKO mice remains incompletely understood. Our data suggest that the enlarged nitrergic neurons in distal small bowel produced excess NO, a neurotransmitter that causes bowel smooth muscle relaxation. Although this could provide a reasonable explanation for the dilated distal small bowels observed in most *Rb1* cKO mice, colon motility defects were also evident and probably contributed to poor growth and early death in these animals. It is possible that the increased number of enteric glia altered motility in small bowel or colon, since glia appear to affect synaptic function, but the role of glia in intestinal motility is still poorly understood (29). Furthermore, there are approximately equal elevations in glial density in the small bowel and colon, implying that increased glial numbers are unlikely to account for both poor contractility in the dilated small bowel and for the abnormal motility in the contracted colon. There is undoubtedly more to learn about how *Rb1* mutations affect ENS function and bowel motility, but the complexity of neural mechanisms that influence bowel function will make this work challenging.

Intestinal pseudo-obstruction and ENS defects have been described in previous studies mating *TyrCre* mice with animals with *Ercc1* floxed alleles (23) or *Pten* floxed alleles (24), consistent with efficient recombination of floxed genes within the ENS with this *Cre*-expressing mouse line, but the expression pattern of the *TyrCre* transgene was not previously well defined. Our analysis shows that the *TyrCre* transgene induces DNA recombination in all enteric glia and most distal small bowel myenteric neurons as well as in a smaller subset of colon myenteric neurons but not in other cells of the bowel wall, supporting the hypothesis that the phenotype observed results from ENS defects.

The ENS phenotype after *Rb1* deletion is complex and reflects the cell-type and context specific roles that RB1 plays in other tissues. RB1 critically regulates the cell cycle by binding to and inhibiting E2F proteins that activate cyclin synthesis. RB1 inactivation should therefore promote cell cycle entry and, if cell division is complete, lead to increased cell number. Remarkably, although *Rb1* is inactivated in *Rb1* cKO mice in many myenteric neuron and glial progenitors, we observed 3 distinct cellular outcomes in many myenteric neuron and glial progenitors. Enteric glia in *Rb1* cKO mice appeared to undergo one additional round of cell division, leading to a 2-fold increase in glia number. Many myenteric neurons, in contrast, did not appear to be affected by *Rb1* inactivation or at least did not enter the cell cycle, as demonstrated by Ki67 staining. However, the most remarkable change occurred within NO-producing myenteric neurons, in which exceptionally large and irregularly shaped nuclei appeared to occur as a result of endoreplication. Endoreplication is a process in which cells go through G_1 and S phases and enter the G_2 phase of the cell cycle but do not undergo mitosis or cytokinesis.

The precise mechanism that induces endoreplication selectively in NO-producing myenteric neurons in *Rb1* cKO mice is unknown. A plausible hypothesis is suggested by the known biological effects of NO and RB1. RB1 loss enhances E2F activity, but this is not enough by itself to induce most postmitotic myenteric neurons to progress through the cell cycle and start DNA replication. However, NO has complex dose-dependent effects, including the activation of AKT and ERK at low levels. In contrast, at high levels, NO induces production of toxic-free radicals (e.g., peroxynitrite anions) that may increase susceptibility of NO neurons to many types of damage (8, 30–32). Interestingly, NO levels in the hippocampus at baseline, (i.e., without activation of NOS) are in the

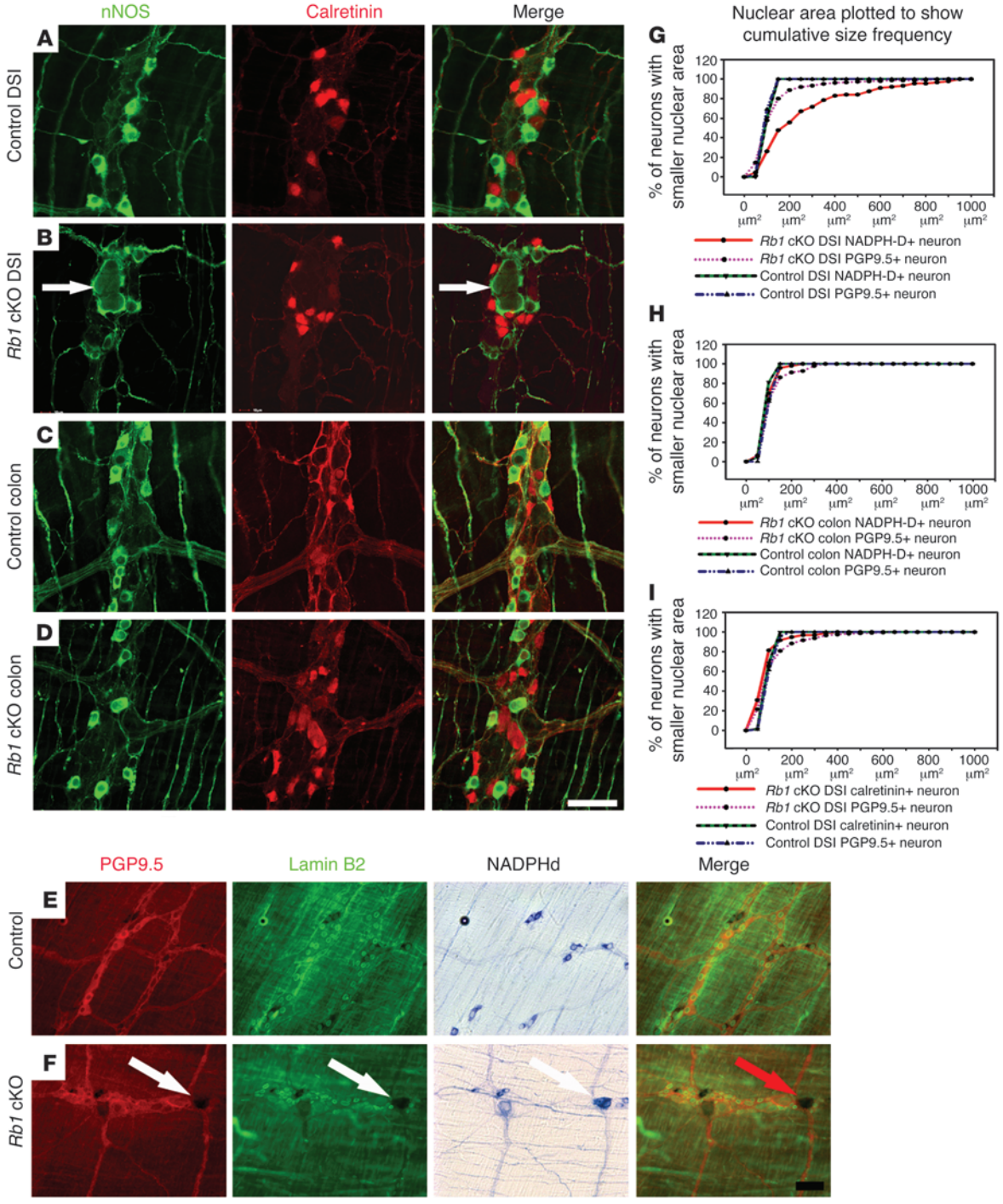

Figure 6

Most giant neurons in distal small bowel myenteric plexus express nNOS. (**A**–**F**) Whole-mount myenteric plexus stained with antibodies to nNOS (green, NO-producing neurons), calretinin (red, excitatory motor neurons), PGP9.5 (red, all neurons), and lamin B2 (green, nuclear lamina) or by NADPH-d histochemistry (NO-producing neurons). (**G**–**I**) Nuclear area for DSI and colon neurons based on lamin B2 staining. Graphs show cumulative frequency for nuclear area. Each point represents the percentage of neurons with nuclear area smaller than the *x* axis value in μm². (**A**–**D**) Typical images of calretinin- and nNOS-expressing neurons in the distal small bowel (**A** and **B**) or colon (**C** and **D**) myenteric plexus of control (**A** and **C**) or*Rb1* cKO (**B** and **D**) mice. (**E** and **F**) Triple labeling for PGP9.5, lamin B2, and NADPH-d in DSIs of control and *Rb1* cKO mice. The arrows highlight a large neuron. (**G**) Quantitative analysis shows that many NADPH-d–expressing neurons have very large nuclei in *Rb1* cKO mice. Since NADPH-d–expressing neurons are common, it is not surprising that enough PGP9.5^{+} neurons have large nuclei to shift the curve. (**H**) Colon myenteric plexus neurons are very close to normal size in *Rb1* cKO mice. (**I**) In contrast to NO-producing neurons, calretinin-expressing myenteric neurons are near normal size in the small intestines of *Rb1* cKO mice. Scale bar: 50 μm. (**G**–**I**) WT, $n = 200$ cells; *Rb1* cKO, $n = 300$ cells per line.

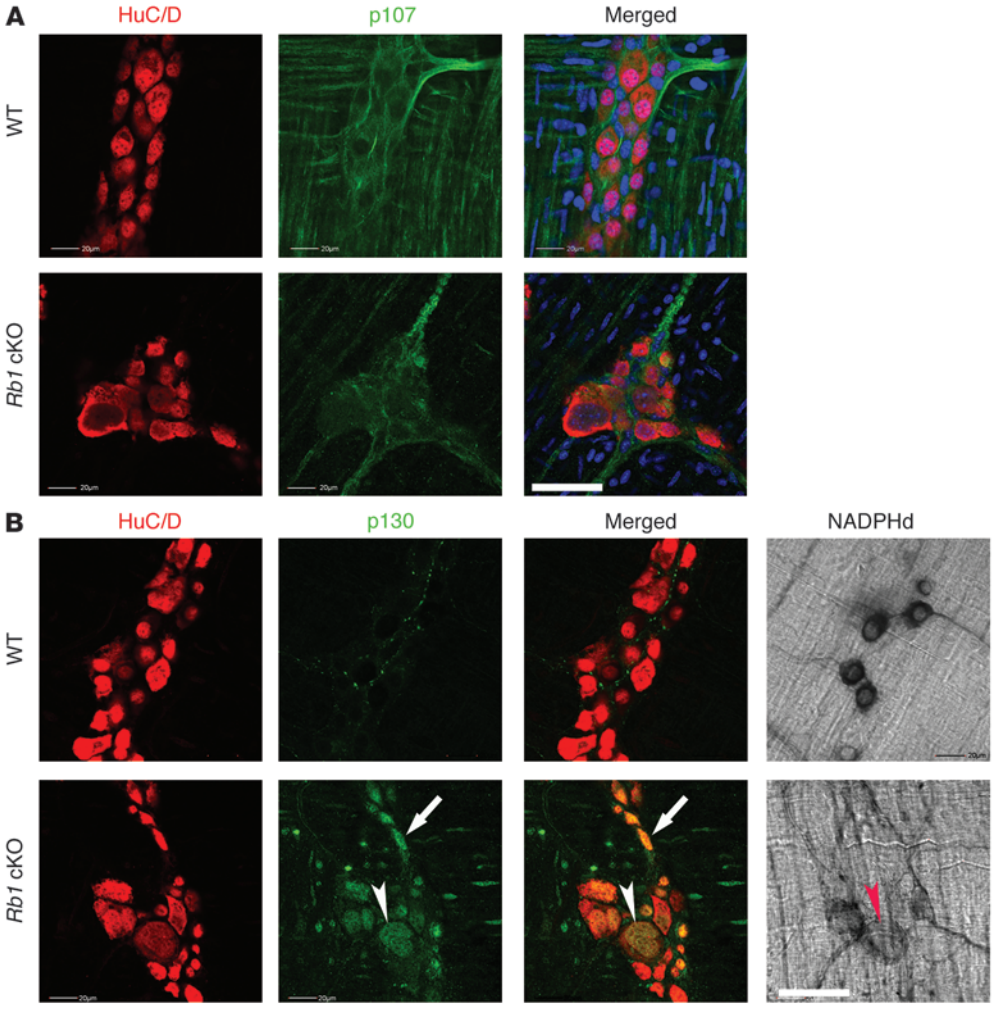

Figure 7
RB1 family members p107 and p130 in the DSI of P30 WT and *Rb1* cKO mice were evaluated by immunohistochemistry. (**A**) p107 immunoreactivity was detected in neurites at a low level but not in neuron cell bodies. (**B**) p130 immunoreactivity was easily detected in all myenteric neurons of the *Rb1* cKO mouse but was difficult to detect in the WT mouse. The white arrows show a myenteric neuron (HuC/D+) that expresses p130 but is not stained with NADPH-d histochemistry. Arrowheads show an NADPH-d histochemistry positive NO-producing neuron that also expresses p130. Scale bar: 50 μm (**A** and **B**, lower right), 20 μm.

range that activates ERK and AKT (30). This may be enough to enhance cell cycle entry in NO-producing neurons but not in adjacent cells that do not produce NO. Consistent with this hypothesis, we demonstrated in vitro that a chemical NO donor increased levels of histone 3 (H3) phosphorylation in ENS precursors. H3 phosphorylation starts in late G_2 phase, increases through late prophase, and continues through metaphase (33). Dephosphorylation of H3 begins in anaphase and ends in telophase. Thus, our results are consistent with the hypothesis that *Rb1*-deficient NO-producing myenteric neurons enter the cell cycle in response to NO and progress to G_2/M but do not complete mitosis, leading to endoreplication and neurons with very large nuclei.

The reason that NO-producing myenteric neurons do not complete mitosis, while enteric glia and many other cell types proliferate in response to *Rb1* loss, is uncertain. However, modeling of the cell cycle using 45 simultaneous differential equations suggests that endoreplication occurs when cells have high levels of the CDH1 (FZR1), an activator of the E3-ubiquitin ligase anaphase-promoting complex (APC) (34). Postmitotic neurons in the central nervous system are known to have high levels of CDH1/APC activity that regulate axon growth and patterning, and prevent cell death (35), but we were unable to obtain good antibodies for immunohistochemistry that would permit colocalization of CDH1 and nNOS within the myenteric plexus. NO-producing neurons may therefore selectively enter the cell cycle because of trophic effects of NO but fail to undergo mitosis, leading to cycles of endoreplication in the setting of high CDH1 levels common in postmitotic neurons.

Our observations fit well with recent studies suggesting that defective RB1 signaling underlies the severe defects in nuclear morphology and aneuploidy seen in several serious human diseases. For example, Hutchinson-Gilford progeria syndrome is caused by mutations in the nuclear intermediate filament protein lamin A (*LMNA*) gene. The most common disease causing mutation (*LMNA* G608G) creates an abnormal splice site, resulting in a 50–amino acid deletion that eliminates a cleavage site for the protease ZMPSTE24 that normally removes the farnesylated and carboxymethylated C terminus of LMNA. LMNA binds directly to hypophosphorylated RB1 during the G_1 phase of the cell cycle and protects RB1 from proteasomal degradation (36). Gene expression profiling of HGPS fibroblasts also demonstrated that *Rb1* mRNA levels are low in HGPS cells and that RB1 is the only known LMNA-interacting protein whose expression is abnormal compared with that of control cells (37). Results of additional studies using a farnesyltransferase inhibitor are consistent with the hypothesis that loss of RB1 is the primary direct effect of the LMNA mutation studied. A major

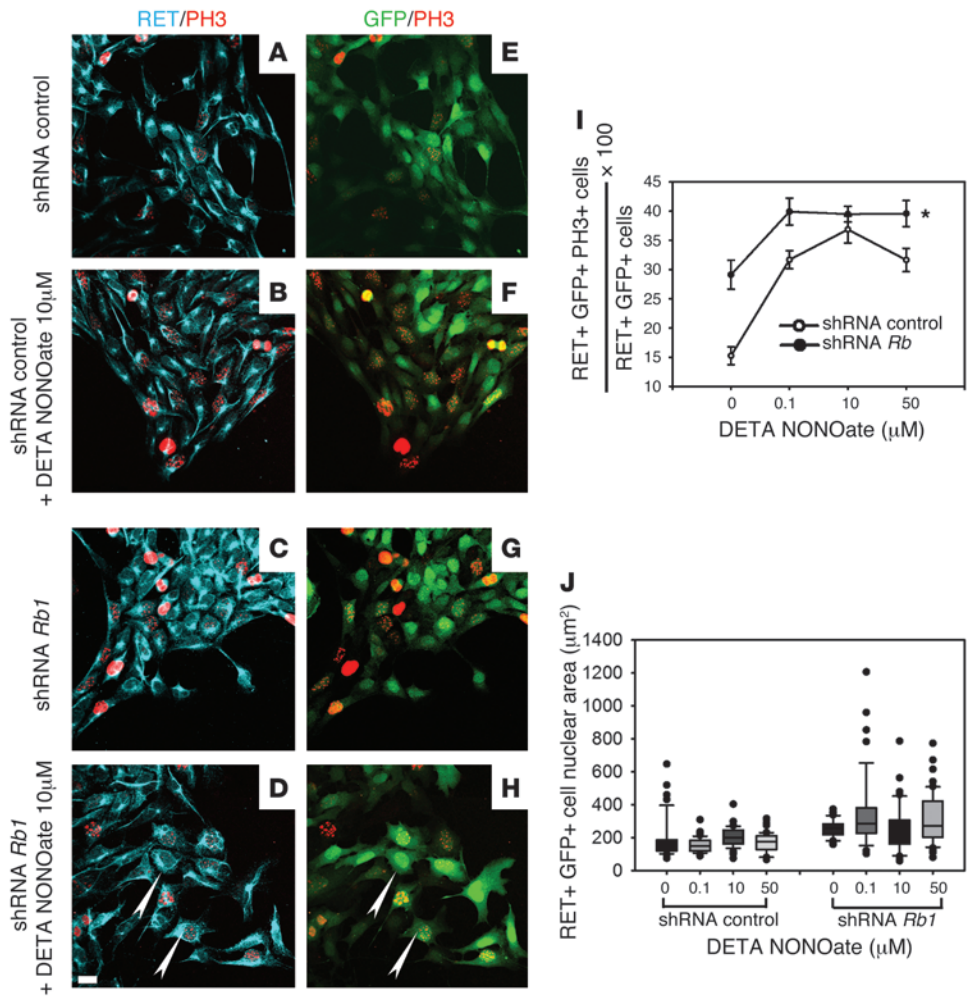

Figure 8
NO donor and *Rb1* silencing increased cell cycle entry in ENS precursors. (**A**–**H**) E12.5 midgut slices were cultured (**B**, **D**, **F**, and **H**) with or (**A**, **C**, **E**, and **G**) without the NO donor DETA NONOate and (**C**, **D**, **G**, and **H**) with lentivirus expressing shRNA against *Rb1* or (**A**, **B**, **E**, and **F**) a control lentivirus for 48 hours. (**D** and **H**) Arrowheads indicate *Rb1* shRNA lentivirus–infected ENS precursors with enlarged nuclei in the presence of NO donor. Antibodies to RET (blue) and PH3 (red) were used to identify neural crest–derived cells and cells in the cell cycle, respectively. (**I**) Quantitative analysis of neural crest–derived (RET^+), virus-infected (GFP^+) cells in the cell cycle ($PH3^+$). (**J**) Quantitative analysis of nuclear area for RET^+GFP^+ cells after virus infection and NO donor or control culture. In box-and-whisker plot, horizontal bars indicate the medians, boxes indicate 25th to 75th percentiles, and whiskers indicate 10th and 90th percentiles. Scale bar: 20 μm. *$P < 0.001$ for *Rb1* shRNA and for DETA NONOate versus controls, 2-way ANOVA.

role for reduced RB1 activity in lamin-related diseases is also suggested by the similar appearance of cells from $Lmna^{Dbe}$ mice to that of the nNOS-expressing myenteric neurons in our *Rb1* cKO animals (38). The $Lmna^{Dbe}$ mutation is a spontaneous semidominant point mutation (L52R) that causes skin and hair changes that are similar to those in human progeria. The mutation is in the coiled-coil domain of lamin proteins and is predicted to disrupt structures needed for self association (39). Defects in nuclear morphology and misregulation of the cell cycle are also reported in association with increased RB1 phosphorylation (i.e., inactivation) in TDP-43 mutant mice (40). TDP-43 mutations occur in people with amyotrophic lateral sclerosis, and TDP-43 aggregates are found in many neurodegenerative diseases. Finally, acute Cre-mediated *Rb1* recombination to delete exon 19 using the same conditional mice that we studied caused increased DNA synthesis, but a block in mitosis in hepatocytes led to cells with 16N ploidy (19), similar to the effect in "postmitotic" NO-producing myenteric neurons. In contrast, acute *Rb1* inactivation in the proliferative cells of the gastrointestinal tract of the same mice led to increased DNA synthesis and increased mitoses without mitotic uncoupling, similar to what we saw in enteric glia. Progression to mitosis depends on cyclin B1 accumulation, and differences in cyclin B1 levels may underlie the differences in cellular response after *Rb1* inactivation. Our studies lend strong support for the hypothesis that many of the LMNA-associated changes in cell cycle control and nuclear morphology are due to reduced RB1 activity.

Summary. *Rb1* cKO mice die prematurely with symptoms of intestinal pseudo-obstruction. These mice have serious defects in ENS structure and intestinal contractility but also have a normal complement of myenteric neurons. The most striking finding is that, while most myenteric neurons have a normal morphologic appearance, many small bowel NO-producing myenteric neurons undergo endoreplication as a result of RB1 loss. We hypothesize that the selective effect of RB1 loss in these cells is a reflection of the unique biochemistry of NO, which promotes cell proliferation and survival at low levels and damages DNA and proteins at high levels. Why the NO-producing neurons with giant nuclei are confined to the small intestine is not known but may reflect differences in NO production or in *Cre* expression in colon and small bowel myenteric neurons. The remarkable similarity in nuclear morphology in small bowel NO-producing myenteric neurons in *Rb1* cKO mice to the enlarged nuclei found in cells with *LMNA* mutations that cause progeria is consistent with a critical role for reduced RB1 activity hypothesized to be important in the pathophysiology of progeria.

Methods

Mice. Characterization of the floxed *Rb1*, *TyrCre*, and *R26REYFP* reporter mice has been reported previously (22, 41, 42). Floxed *Rb1* ($Rb1^{fl/fl}$) mice

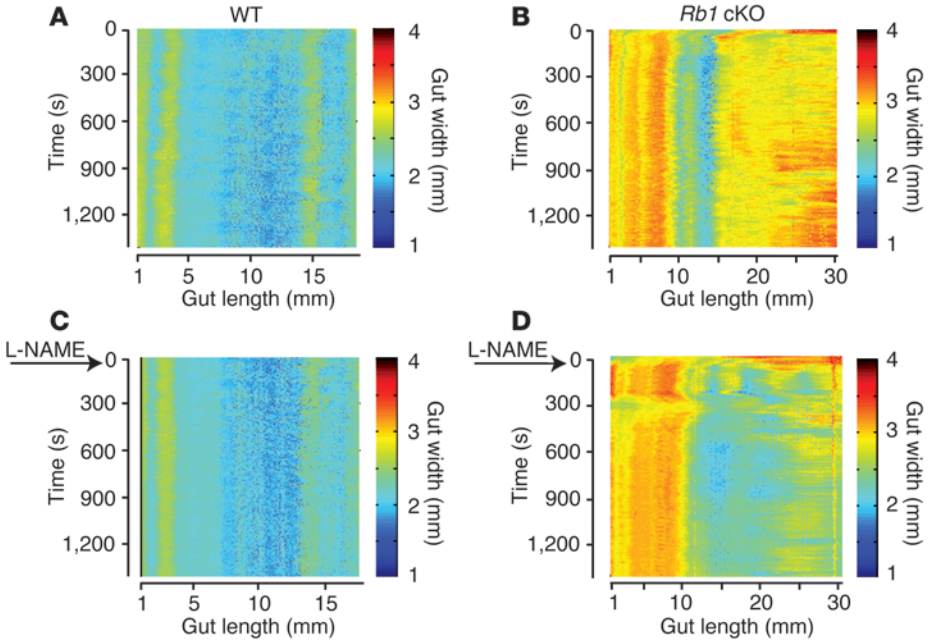

Figure 9
Rb1 cKO distal small bowel contractility is abnormal. (**A** and **B**) Kymographs were generated from video images of (**A**) a WT and (**B**) a mildly affected *Rb1* cKO mouse distal small bowel maintained in an oxygenated organ bath. Bowel lumen was not perfused or stimulated during video imaging. Mutant bowel was dilated compared with WT bowel. (**C** and **D**) The same segments of bowel as in **A** and **B** are shown but with NOS inhibitor L-NAME added within 15 seconds of recording (arrows). Kymographs show the width of the bowel (via color coding) at a particular position (*x* axis) and a particular time (*y* axis). Proximal bowel is on the left.

were obtained from the National Cancer Institute Mouse Repository (strain 01XC1; Frederick, Maryland, USA). This strain carries a conditional mutation in the endogenous *Rb1* gene, with LoxP sites inserted into introns surrounding exon 19 (41). Mice with a tyrosinase promoter driving *Cre* expression (*TyrCre* mice) were provided by Graham F. Kay (Queensland Institute of Medical Research, Herston, Queensland, Australia) (22). *R26REYFP* reporter mice (B6.129X1-*Gt[ROSA]26Sor*$^{tm1[EYFP]Cos}$/J) were used to monitor expression of the *Cre* transgene (The Jackson Laboratory; C57BL/6J background) (42). *TyrCre*$^{+}$ mice (C57BL/6J background) were crossed with floxed *Rb1* mice (FVB/129 background), which were subsequently interbred for 5 to 7 generations to generate *Rb1* cKO mice, *TyrCre*$^{+}$;*Rb1*$^{fl/+}$ (conditional heterozygous *Rb1* cKO) mice, and control mice that either lack Cre or lack floxed *Rb1* alleles. Mice were genotyped for *Cre*, *Rb1*, or *GFP* by PCR analyses, as previously described, using DNA extracted from tail or ear biopsies (22, 41). For timed pregnancies, the day on which the vaginal plug was detected was considered E0.5. Survival curves were determined by Kaplan-Meier analysis for *Rb1*$^{+/+}$ and *Rb1*$^{fl/fl}$ animals carrying the *TyrCre* transgene (i.e., control and *Rb1* cKO animals).

Myenteric whole-mount preparations. Mice were euthanized by carbon dioxide asphyxiation (adult) or cervical dislocation (<P14). The gastrointestinal tract was removed, flushed with ice-cold PBS, opened by cutting along the mesenteric border, flattened, and pinned mucosal side down on Sylgard dishes. After fixation with 4% paraformaldehyde (30 minutes), muscle layers containing myenteric plexus were separated from mucosa and submucosa using fine-pointed forceps under a dissecting microscope. Samples from DSI and colon were cut into 1-cm segments and stored in 50% glycerol/PBS at –20°C until staining and analysis.

Whole-mount immunohistochemistry. Myenteric whole-mount preparations were permeabilized and blocked with 10% donkey serum/TBST (100 mM Tris, 150 mM NaCl, 1% Triton X-100) for 1 hour and then incubated for 18 hours at 4°C (or 2 hours at 37°C for lamin antibodies) with the following primary antibodies: mouse biotinylated-HuC/D (1:250; Invitrogen), rabbit TuJ1 (1:10,000; Covance), goat SOX10 (1:250; Santa Cruz Biotechnology Inc.), goat LMNA/C (1:250; Santa Cruz Biotechnology Inc.), mouse lamin B2 (1:250; Invitrogen), rabbit PGP9.5 (1:500; AbD Serotec), rabbit S100 (1:1,000; DAKO), rabbit Ki67 (1:250; Abcam), Alexa Fluor 488 conjugated to anti-BrdU mouse monoclonal antibody (1:100; Invitrogen), goat calretinin (1:250; Chemicon), rabbit nNOS (1:250; Chemicon), rabbit γH2AX (1:400; Bethyl Laboratories), PHOX2B (1:10,000, a gift from J.F. Brunet, Institut de Biologie de l'École Normale Supérieure, Paris, France), rabbit p107 (C-18) (1:50; Santa Cruz Biotechnology Inc.), rabbit p130 (C-20) (1:50; Santa Cruz Biotechnology Inc.), goat RET (1:100; Neuromics), and rabbit PH3 (S10) (1:100; Cell Signaling). Donkey secondary antibodies used were Alexa Fluor 488, 594, or 647 (1:500; Invitrogen). Nuclei were counterstained with DRAQ5 (1:2,000; Cell Signaling) or DAPI. TUNEL assay was performed with the In Situ Cell Death Detection TMR Red Kit (Roche Applied Science; positive control: DNase I treatment). Specimens were mounted on slides in 50% glycerol in PBS and

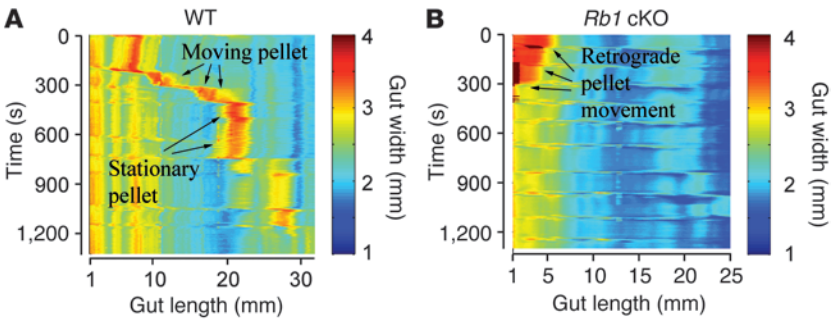

Figure 10
Rb1 cKO mouse colon contracts abnormally. Colon was maintained in an oxygenated organ bath. An artificial stool pellet was inserted into proximal colon (left). Kymographs show colon width (by a color code) at specific positions (*x* axis) and times (*y* axis). (**A**) WT colon propelled the pellet distally, (**B**) but *Rb1* cKO colon expelled the pellet from the proximal end.

observed using upright laser scanning confocal microscopes (Zeiss LSM 510 and Olympus FV1000). Tissue specimens were excited using argon (488 nm), $HeNe_1$ (543 nm), and $HeNe_2$ (633 nm) lasers, with excitation and barrier filters set for individual fluorophores according to their specific excitation/emission spectra (λ = 488 nm, 594 nm, 647 nm). The detection pinhole was set for use with different objectives accordingly. Offset and gain settings were determined at the start of each experiment and kept constant throughout, with laser power recorded each time.

Reduced NADPH-d staining. NO-producing inhibitory neurons were visualized in myenteric whole-mount preparations using NADPH-d staining (43). Stained samples were examined under a bright-field microscope, and neurons were counted using a 1.0 × 1.0 mm^2 grid counting eyepiece (×10 objective). Twenty randomly selected fields were counted for each region, and data are presented as neurons per mm^2. Contrast and brightness of digital images were uniformly adjusted with Photoshop.

Nuclear size analysis. Nuclear size of total myenteric, calretinin-expressing, and NO-producing neurons was determined by triple labeling with NADPH-d, lamin B2, and PGP9.5 or with calretinin, lamin B2, and PGP9.5 antibodies. A plug-in from ImageJ was used for nuclear area measurements (μm^2), and distribution was plotted as cumulative frequency (%).

BrdU incorporation. Mice were injected with BrdU (100 μg; Invitrogen) intraperitoneally once daily from P9 to P16 and then analyzed at P20. Myenteric whole-mount preparations were permeabilized in 0.5% Triton-X100 in PBS for 1 hour. DSI and colon were then stained for BrdU using an Alexa Fluor 488 anti-BrdU mouse monoclonal antibody (1:100; Invitrogen) for 1 hour at 37°C according to the manufacturer's instructions. Stained samples were washed before blocking with 10% donkey serum/TBST for 1 hour and then incubated for triple labeling with PGP9.5 antibody (followed by donkey anti-rabbit Alexa Fluor 594) and SOX10 antibody (followed by donkey anti-goat Alexa Fluor 647). Specimens were mounted in 50% glycerol in PBS. $PGP9.5^+/BrdU^+$ and $SOX10^+/BrdU^+$ (WT mice, n = 4; Rb1 cKO mice, n = 5) cells were counted in 10 fields for each region per mouse (DSI and colon). Fields were randomly selected using PGP9.5 staining.

DNA content analysis. DSI tissue specimens were stained with lamin B2 antibody to delineate the nuclear lamina of the myenteric neurons. Nuclei were then counterstained with DRAQ5 to determine their DNA content (stoichiometric DNA binding; 1:2,000; 12 hours at 4°C). Z-stacks of myenteric plexuses were recorded using an upright laser scanning confocal microscope (Zeiss LSM 510) with a water immersion ×40 objective (0.5-μm-thick slices; 8–10 Z-stacks; 30–67 cells per animal). Measure Stack.java software (OptiNav Inc.) downloaded to the ImageJ plug-ins folder was used for measurements on a series of slices from Z-stacks. The results were summed to determine the nuclear volume (log_2) and DRAQ5 intensity (log_2; mean gray value of pixels within the nucleus)

Rb1 shRNA. The shRNA plasmid DNA used to generate *Rb1* and control vectors was created by the RNAi core of Washington University in St. Louis using the vector pLKO.1-puro that also encodes a puromycin resistance gene (44). The *Rb1* target sequence is GCAGTGCGTTATCTACTGAAA. The control target sequence is CGTCGTATTACAACGTCGTGA. The puromycin resistance gene was replaced with EGFP from pBK-CMV using Bamh1 and KpnI to digest both vectors.

Lentivirus production. To produce *Rb1* and control shRNA-expressing lentivirus, the plasmids pLKO.1 Rb1 EGFP or pLKO.1 control EGFP (1 μg) plus Δ8.9 (0.89 μg; BD Biosciences) and VSV-G (0.11 μg; BD Biosciences) were mixed in 50 μl DMEM plus FuGENE 6 (6 μl per well) for 30 minutes at room temperature. The plasmid mixture was added to HEK293T cells in 30-mm dishes (6-well dishes). Medium was replaced with 2 ml fresh DMEM plus chicken embryo extract (10%) 16 hours after transfection. The culture supernatants with virus particles were collected after 48 hours. To eliminate the cell debris, supernatant was centrifuged for 10 minutes at 4°C at 500 × *g*, filtered with a 0.22-μm syringe top filter, and stored in aliquots at –80°C until use.

qRT-PCR. Bowel from E12.5 CF-1 mouse was dissociated with dispase and collagenase and cultured as described previously (45). Lentivirus was added after 16 hours of culture. Medium was replaced after 24 hours, and cells were collected for RNA purification 48 hours after virus addition. Reverse transcription was carried out using 10 ng total RNA and SuperScript III (Invitrogen) following the manufacturer's protocol. Fast SYBR Green Master Mix (Applied Biosystems) was used to quantify relative *Rb1* mRNA levels by qRT-PCR with a Mx3005P (Agilent Technologies) instrument and *Rb1* primers (forward 5′CCTTGAACCTGCTTGTCCTC3′, reverse 5′TGAGGCTGCTTGTGTCTCTG3′) as well as GAPDH primers (forward 5′AACTTTGGCATTGTGGAAGG3′, reverse 5′ GGATGCAGGGATGATGTTCT3′).

ENS precursor culture for Rb1 shRNA and DETA NONOate studies. E12.5 mouse midgut slices (300- to 400-μm thick) were cultured on fibronectin-coated (250 μg/ml; GIBCO) 8-well glass chamber slides (NUNC, catalog no. 177402) in DMEM with chicken embryo extract (10% chicken embryo extract; Seralab); N2 (1%; Invitrogen); B27 (2%; Invitrogen); bFGF (20 ng/ml; R&D Systems); EGF (20 ng/ml; Calbiochem); retinoic acid (35 ng/ml; Sigma-Aldrich); and β-mercaptoethanol (50 μM; Sigma-Aldrich). Four hours after plating, GDNF was added (50 ng/ml) to induce enteric neural crest–derived cell migration from the slice. Sixteen hours later, cultures were treated with control virus (5×10^6 CFU/ml) or *Rb1* shRNA virus (2×10^6 CFU/ml) containing medium and DETA NONOate (Cayman). Medium was replaced with fresh DMEM, chicken embryo extract, and DETA NONOate after 24 hours, and cultures were fixed (30 minutes at 25°C) in 4% paraformaldehyde 48 hours after virus and DETA NONOate addition.

Functional motility analysis. DSIs and colons from *Rb1* cKO and WT littermates were pinned to Sylgard and maintained in a 37°C water bath with 20 ml oxygenated (95% O_2 and 5% CO_2) physiological saline solution of the following composition: 1x Krebs buffer (Sigma-Aldrich, product no. K4002) with additional D-glucose 2 g/l, $NaHCO_3$ 2.1 g/l, and $CaCl_2$ 0.28 g/l. The saline was continuously superfused through the organ bath at a flow rate of 15 ml/min. After 30 minutes equilibration, an artificial pellet was placed at the proximal end of the colon. Video images were recorded for 25 minutes before adding a NOS blocker (100 μM L-NAME) (Cayman) to the water bath.

Video imaging. Video images were captured at ×0.67 optical magnification with an E-PM1 Olympus digital video camera mounted on a dissecting microscope (15 frames per second, 1,920 × 1,080 pixels resolution). AVIDEMUX version 2.6.1 software was used to convert MTS to Avi format. Then, files were converted from Avi to SU2 format using software (Scribble v.2) provided by Joel C. Bornstein (Department of Physiology, University of Melbourne, Parkville, Victoria, Australia). Finally, spatiotemporal maps were generated and analyzed with custom software (Analyze) also developed by Joel C. Bornstein's group using MATLAB 7.0.4. (46).

Measurement of NO synthesis in bowel muscle layers. The small intestine from 10 cm distal to the stomach to 10 cm proximal to the cecum was dissected in oxygenated 1× Krebs buffer (Sigma-Aldrich, product no. K4002) with additional 2 g/l D-glucose, 2.1 g/l $NaHCO_3$, and 0.28 g/l $CaCl_2$ to separate smooth muscle layers, including the myenteric plexus from submucosa and mucosa. These muscle layers were incubated in L-[^{3}H] arginine (3 μCi/ml; PerkinElmer) at 37°C for 15 minutes to permit conversion of arginine to citrulline and NO. Tissue was flash frozen in liquid nitrogen and stored at –80°C until analysis. L-[^{3}H] citrulline was extracted by homogenizing weighed muscle preparations (Dounce homogenizer) and precipitating protein with 1 M trichloroacetic acid (Sigma-Aldrich), water/ether extraction (×3), and column chromatography (Dowex AG50WX-8 [Sigma-Aldrich] Na+form) as described previously (26) before scintillation counting.

Statistics. Student's *t* test was used when comparing WT mice to *Rb1* cKO mice. For studies in which enteric neural crest–derived cells were treated

with *Rb1* shRNA and DETA NONOate in vitro, a 2-way ANOVA was performed. Data were analyzed for statistical significance using MedCalc software version 9.5.1.0 (http://medcalcsoftware.com/medcalc.php), R version 2.15 (R Foundation), or SigmaPlot version 11.2. For all studies, the sample size included 3 or more mice for each genotype. The values are represented as mean ± SEM, and $P < 0.05$ was considered significant.

Study approval. The Animal Studies Committee of Washington University School of Medicine in St. Louis approved all experiments with animals.

Acknowledgments

The authors would like to thank Graham F. Kay (Queensland Institute of Medical Research, Australia) for providing *TyrCre* mice, Suellen C. Greco from Division of Comparative Medicine for animal pathology reports, Frank E. Schottler in the Immunomorphology Core Lab for his technical help with confocal microscopy, Richard Heil-Chapdelaine for expert guidance generating confocal 3-dimensional images, and Susana Gonzalo for helpful advice on lamin proteins. We also thank S. Celeste Morley and Elizabeth Todd for help with γ-irradiation, Werend Boesmans and Joel Bornstein for expert guidance on intestinal motility testing and for sharing software, Allan Doctor and John R. Grider for advice on NO analyses, and Jonathan Lake for assistance with motility studies and statistical analyses. This work was supported by Fonds de la Recherche du Québec-Santé Postdoctoral Training Award (to S. Landreville), Knights Templar Eye Foundation Postdoctoral Research Fellowship (to L. Wiley), Children's Discovery Institute CDI-FR-2011-145 (to M. Shoykhet), Scholar of the Child Health Research Center at Washington University School of Medicine in St. Louis K12-HD076224 (to M. Shoykhet), NIH KO8 NS082362-01 (to M. Shoykhet), NIH R01 DK087715 and R01 DK57038 (to R.O. Heuckeroth), Burroughs Wellcome Fund Clinical Scientist Award in Translational Research 1008525 (to R.O. Heuckeroth), Children's Discovery Institute of Washington University and St. Louis Children's Hospital (CH-II-1008-123 and CH-II-2013-269) (to R.O. Heuckeroth), NIH R01 EY13169 (to J.W. Harbour), Research to Prevent Blindness (to J.W. Harbour), and an unrestricted grant to the Department of Ophthalmology and Visual Sciences from Research to Prevent Blindness Inc., and the NIH Vision Core grant P30 EY02687. The Washington University RNAi core is supported by the Children's Discovery Institute of Washington University and St. Louis Children's Hospital (CDI-LI-2010-94), The RNAi Consortium (TRC), and The Genome Institute at Washington University (TGI).

Received for publication November 1, 2012, and accepted in revised form August 15, 2013.

Address correspondence to: J. William Harbour, Bascom Palmer Eye Institute, Sylvester Comprehensive Cancer Center, University of Miami Miller School of Medicine, 900 N.W. 17th Street, Miami, Florida 33136, USA. Phone: 305.326.6166; Fax: 305.326.6417; E-mail: jwharbour@med.miami.edu. Or to: Robert O. Heuckeroth, Irma and Norman Braman Endowed Chair for Research in GI Motility Disorders, The Children's Hospital of Philadelphia Research Institute, 3615 Civic Center Blvd., Abramson Research Center — Suite #1116I, Philadelphia, Pennsylvania 19104-4318, USA. Phone: 215.590.1209; Fax: 215.590.3324; E-mail: HeuckerothR@email.chop.edu.

Robert O. Heuckeroth's present address is: Irma and Norman Braman Endowed Chair for Research in GI Motility Disorders, The Children's Hospital of Philadelphia Research Institute, Philadelphia, Pennsylvania, USA.

1. O'Keefe SJ, Matarese L. Small bowel transplantation. *Curr Gastroenterol Rep*. 2006;8(5):360–366.
2. Sasselli V, Pachnis V, Burns AJ. The enteric nervous system. *Dev Biol*. 2012;366(1):64–73.
3. Furness JB. *The Enteric Nervous System*. Malden, Massachusetts, USA: Blackwell Publishing; 2006.
4. Grundy D, Schemann M. Enteric nervous system. *Curr Opin Gastroenterol*. 2005;21(2):176–182.
5. Newgreen D, Young HM. Enteric nervous system: development and developmental disturbances — part 1. *Pediatr Dev Pathol*. 2002;5(3):224–247.
6. Heanue TA, Pachnis V. Enteric nervous system development and Hirschsprung's disease: advances in genetic and stem cell studies. *Nat Rev Neurosci*. 2007; 8(6):466–479.
7. Goldstein A, Hofstra R, Burns A. Building a brain in the gut: development of the enteric nervous system. *Clin Genet*. 2012;83(4):307–316.
8. Rivera LR, Poole DP, Thacker M, Furness JB. The involvement of nitric oxide synthase neurons in enteric neuropathies. *Neurogastroenterol Motil*. 2011; 23(11):980–988.
9. Viader A, Wright-Jin EC, Vohra BP, Heuckeroth RO, Milbrandt J. Differential regional and subtype-specific vulnerability of enteric neurons to mitochondrial dysfunction. *PLoS One*. 2011;6(11):e27727.
10. Burkhart DL, Sage J. Cellular mechanisms of tumour suppression by the retinoblastoma gene. *Nat Rev Cancer*. 2008;8(9):671–682.
11. Delston RB, Matatall KA, Sun Y, Onken MD, Harbour JW. p38 phosphorylates Rb on Ser567 by a novel, cell cycle-independent mechanism that triggers Rb-Hdm2 interaction and apoptosis. *Oncogene*. 2011; 30(5):588–599.
12. Lundberg AS, Weinberg RA. Functional inactivation of the retinoblastoma protein requires sequential modification by at least two distinct cyclin-cdk complexes. *Mol Cell Biol*. 1998;18(2):753–761.
13. Harbour JW, Luo RX, Dei Santi A, Postigo AA, Dean DC. Cdk phosphorylation triggers sequential intramolecular interactions that progressively block Rb functions as cells move through G1. *Cell*. 1999; 98(6):859–869.
14. Genovese C, Trani D, Caputi M, Claudio PP. Cell cycle control and beyond: emerging roles for the retinoblastoma gene family. *Oncogene*. 2006; 25(38):5201–5209.
15. Lipinski MM, Jacks T. The retinoblastoma gene family in differentiation and development. *Oncogene*. 1999;18(55):7873–7882.
16. Slack RS, Miller FD. Retinoblastoma gene in mouse neural development. *Dev Genet*. 1996;18(1):81–91.
17. Goodrich DW, Wang NP, Qian YW, Lee EY, Lee WH. The retinoblastoma gene product regulates progression through the G1 phase of the cell cycle. *Cell*. 1991;67(2):293–302.
18. Sage J, Miller AL, Perez-Mancera PA, Wysocki JM, Jacks T. Acute mutation of retinoblastoma gene function is sufficient for cell cycle re-entry. *Nature*. 2003;424(6945):223–228.
19. Bourgo RJ, Ehmer U, Sage J, Knudsen ES. RB deletion disrupts coordination between DNA replication licensing and mitotic entry in vivo. *Mol Biol Cell*. 2011;22(7):931–939.
20. Loercher AE, Tank EM, Delston RB, Harbour JW. MITF links differentiation with cell cycle arrest in melanocytes by transcriptional activation of INK4A. *J Cell Biol*. 2005;168(1):35–40.
21. Tonks ID, et al. Melanocyte homeostasis in vivo tolerates Rb1 loss in a developmentally independent fashion. *Pigment Cell Melanoma Res*. 2010;23(4):564–570.
22. Tonks ID, et al. Tyrosinase-Cre mice for tissue-specific gene ablation in neural crest and neuroepithelial-derived tissues. *Genesis*. 2003;37(3):131–138.
23. Selfridge J, Song L, Brownstein DG, Melton DW. Mice with DNA repair gene Ercc1 deficiency in a neural crest lineage are a model for late-onset Hirschsprung disease. *DNA Repair (Amst)*. 2010; 9(6):653–660.
24. Puig I, Champeval D, De Santa Barbara P, Jaubert F, Lyonnet S, Larue L. Deletion of Pten in the mouse enteric nervous system induces ganglioneuromatosis and mimics intestinal pseudoobstruction. *J Clin Invest*. 2009;119(12):3586–3596.
25. Sang Q, Williamson S, Young HM. Projections of chemically identified myenteric neurons of the small and large intestine of the mouse. *J Anat*. 1997; 190(pt 2):209–222.
26. Bredt DS, Snyder SH. Nitric oxide mediates glutamate-linked enhancement of cGMP levels in the cerebellum. *Proc Natl Acad Sci U S A*. 1989; 86(22):9030–9033.
27. Weigel BJ, Pierpont ME, Young TL, Mutchler SB, Neglia JP. Retinoblastoma and Hirschsprung disease in a patient with interstitial deletion of chromosome 13. *Am J Med Genet*. 1998;77(4):285–288.
28. Sparkes RS, Sparkes MC, Kalina RE, Pagon RA, Salk DJ, Disteche CM. Separation of retinoblastoma and esterase D loci in a patient with sporadic retinoblastoma and del(13)(q14.1q22.3). *Hum Genet*. 1984;68(3):258–259.
29. Gulbransen BD, Sharkey KA. Novel functional roles for enteric glia in the gastrointestinal tract. *Nat Rev Gastroenterol Hepatol*. 2012;9(11):625–632.
30. Lourenco CF, Santos R, Barbosa RM, Gerhardt G,

Cadenas E, Laranjinha J. In vivo modulation of nitric oxide concentration dynamics upon glutamatergic neuronal activation in the hippocampus. *Hippocampus*. 2011;21(6):622–630.
31. Thomas DD, et al. The chemical biology of nitric oxide: implications in cellular signaling. *Free Radic Biol Med*. 2008;45(1):18–31.
32. Carreira BP, et al. Nitric oxide stimulates the proliferation of neural stem cells bypassing the epidermal growth factor receptor. *Stem Cells*. 2010; 28(7):1219–1230.
33. Hans F, Dimitrov S. Histone H3 phosphorylation and cell division. *Oncogene*. 2001;20(24):3021–3027.
34. Gerard C, Goldbeter A. Temporal self-organization of the cyclin/Cdk network driving the mammalian cell cycle. *Proc Natl Acad Sci U S A*. 2009; 106(51):21643–21648.
35. Almeida A, Bolanos JP, Moreno S. Cdh1/Hct1-APC is essential for the survival of postmitotic neurons. *J Neurosci*. 2005;25(36):8115–8121.
36. Johnson BR, et al. A-type lamins regulate retinoblastoma protein function by promoting subnuclear localization and preventing proteasomal degradation. *Proc Natl Acad Sci U S A*. 2004; 101(26):9677–9682.
37. Marji J, et al. Defective lamin A-Rb signaling in Hutchinson-Gilford Progeria Syndrome and reversal by farnesyltransferase inhibition. *PLoS One*. 2010; 5(6):e11132.
38. Pratt CH, Curtain M, Donahue LR, Shopland LS. Mitotic defects lead to pervasive aneuploidy and accompany loss of RB1 activity in mouse LmnaDhe dermal fibroblasts. *PLoS One*. 2011;6(3):e18065.
39. Odgren PR, et al. Disheveled hair and ear (Dhe), a spontaneous mouse Lmna mutation modeling human laminopathies. *PLoS One*. 2010;5(4):e9959.
40. Ayala YM, Misteli T, Baralle FE. TDP-43 regulates retinoblastoma protein phosphorylation through the repression of cyclin-dependent kinase 6 expression. *Proc Natl Acad Sci U S A*. 2008;105(10):3785–3789.
41. Marino S, Vooijs M, van Der Gulden H, Jonkers J, Berns A. Induction of medulloblastomas in p53-null mutant mice by somatic inactivation of Rb in the external granular layer cells of the cerebellum. *Genes Dev*. 2000;14(8):994–1004.
42. Srinivas S, et al. Cre reporter strains produced by targeted insertion of EYFP and ECFP into the ROSA26 locus. *BMC Dev Biol*. 2001;1:4.
43. Neuhuber WL, Worl J, Berthoud HR, Conte B. NADPH-diaphorase-positive nerve fibers associated with motor endplates in the rat esophagus: new evidence for co-innervation of striated muscle by enteric neurons. *Cell Tissue Res*. 1994;276(1):23–30.
44. Moffat J, et al. A lentiviral RNAi library for human and mouse genes applied to an arrayed viral high-content screen. *Cell*. 2006;124(6):1283–1298.
45. Sato Y, Heuckeroth RO. Retinoic acid regulates murine enteric nervous system precursor proliferation, enhances neuronal precursor differentiation, and reduces neurite growth in vitro. *Dev Biol*. 2008; 320(1):185–198.
46. Roberts RR, Murphy JF, Young HM, Bornstein JC. Development of colonic motility in the neonatal mouse-studies using spatiotemporal maps. *Am J Physiol Gastrointest Liver Physiol*. 2007; 292(3):G930–G938.